ROUTE PLANNING FOR VOLCANIC ASH AND RADIOACTIVITY IN-SITU DRONE MEASUREMENTS USING A GENETIC ALGORITHM AND KRIGING

Kuno A. Buchtal[1], Alexander Lau[1], Dörthe Ebert[2], Jochen Richters[2] & Kilian Schneiders[2]

[1]German Aerospace Center (DLR), Institute of Air Transport, Hamburg, Germany
[2]DWD German Weather Service, Radioactivity Monitoring, Offenbach, Germany

Abstract

This study presents a methodology for optimizing route planning for Unmanned Aerial Systems (UAS) conducting in-situ measurements of volcanic ash and radioactivity. Utilizing a genetic algorithm combined with Kriging, this approach aims to enhance the optimization of measurement routes for improved in-situ data collection in contaminated airspaces. The genetic algorithm optimizes routes to minimize the mean absolute error of Kriging estimates against reference data while adhering to mission constraints. An ICON-ART atmospheric model system provides the propagation information for the contamination scenario serving as the basis for route optimization. Results demonstrate the effectiveness of the approach by flexible but shorter measurement routes comparing against a standard coverage pattern. This study contributes to the advancement of UAS path planning for environmental monitoring and disaster response.

Keywords: Route planning, UAS, Kriging, Genetic Algorithm, In-situ measurements

1. Introduction

The presence of atmospheric events with corresponding contamination relevant to flight safety, such as volcanic and radioactive radiation, have a relevant effect on air traffic operations. One of the biggest events of this kind in Europe was the eruption of Eyjafjallajökull in Iceland in 2010. More than 10 million passengers were stranded, and airlines lost more than $1.7 billion in revenue [1]. The incident showed a significant lack of volcanic monitoring information for airborne hazards [2].

The Horizon 2020 research project EUNADICS-AV (European Natural Disaster Coordination and Information System for Aviation, 2016–2019) was setting up an early warning system (EWS) to combine data from satellite, ground-based instrumentation and in-situ data sources collectively, and visualize those on a dedicated platform. The goal was to provide all stakeholders in aviation with high-quality information and alerts during airborne hazards (volcanic, dust, smoke and radionuclide clouds) [3]. Automated in-situ measurements of the system include the monitoring of seismic activity and volcanic tremor reported by the Volcano Observatory Notice for Aviation (VONA) for volcanic hazards. In-situ radiological data are obtained by the European Radiological Data Exchange Platform (EURDEP), which provides gamma dose rates and Nuclide concentrations in ground-level air [4]. Both institutions provide ground-based measurements, so airborne measurements are still missing in the event of this kind.

The collaborative project MEASURE, funded by German Federal Aeronautical Research Programme ‘Luftfahrtforschungsprogamm’, LuFo), and led by DWD German Weather Service, is set up to build, test and verify the operation of a remotely piloted aircraft system (RPAS) for in-situ airborne measurements of particles and radiological data in case of a contamination event to maintain safety in the airspace. On-board measuring systems for in-situ measurements, as well as a data link for air-to-ground data transmission is designed and integrated into an existing RPAS platform within the scope of the project. A suitable RPAS platform needs to fulfill dedicated mission requirements, like payload,

maximum range, operating altitude as well as necessary certification requirements for planned missions. The testplatform Airbus DO-TP 25, which is shown in Figure 1, meets these requirements and has therefore been selected within the project. Key specifications are displayed in Table 1.
In-situ measurements provide real-time data to update and verify these forecasts of the contamination propagation. Scope of this paper is to show and test a methodology to generate flight routes for a best-possible measurement data collection in a contaminated airspace.

Figure 1 – DO-TP 25 – Remotely piloted aircraft system [5].

Table 1 – Flight performance data.

Performance parameters	@ SL, ISA
Maximum speed	300 kts (154 m/s)
Endurance	60 min (mixed speed)
Operating Altitude	35 – 30,000 ft (10 – 9144 m)
Operating Range	110 km LoS

2. Related Work

Unmanned Aerial Systems (UAS), a broad category that includes various types of unmanned aircraft, encompass Remotely Piloted Aircraft Systems (RPAS) as a specific subset. While RPAS are a key focus in this study, the literature on UAS path planning is highly relevant and provides valuable insights applicable to RPAS as well. This section provides an overview of UAS path planning, categorizing it into offline (pre-flight) and online (in-flight) approaches as well as 2D and 3D methods, highlighting the multi-objective nature of these path planning problems. Furthermore, the role of genetic algorithms (GA) in both, offline and online path planning, is explored, emphasizing their suitability in terms of robustness and adaptability in dynamic environments. Finally, the concept of informative path planning and its usage in environmental monitoring and exploration is shown. This includes the integration of geostatistical methods like Kriging for efficient data collection.

2.1 UAS Path Planning

UAS have become integral to numerous industries, including logistics, environmental monitoring, and data collection [6]. UAS path planning is essential for optimizing routes that allow drones to complete tasks efficiently, considering factors such as operating costs, time, and energy consumption [7]. Offline path planning involves pre-determined routes calculated before the UAS starts its mission, making it suitable for environments that are well-mapped and predictable [8]. In contrast, online path planning is dynamic, allowing UAS to adapt to real-time changes and unforeseen obstacles in their environment [9] in terms of an in-flight separation management.
Many UAS path planning problems are multi-objective, requiring the simultaneous optimization of several goals such as minimizing travel time and energy consumption while maximizing coverage and information gain [10, 11]. Balancing these objectives is crucial for the efficiency and effectiveness of UAS operations. Therefore, *informative* path planning involves creating paths that maximize the information gathered about an environment, particularly valuable in tasks such as environmental monitoring, where UAS equipped with sensors collect high-resolution, real-time data [12]. This plays

a special role in disaster response scenarios, in which sensor-equipped UAS can provide detailed assessments of affected areas and airpsaces, enhancing the speed and accuracy of relief efforts [13].
Spatial domain-based classification distinguishes UAS path planning methods into 2D and 3D approaches, depending on whether flight altitude is taken into account during planning. Generic algorithms show good performance on multi-objective problems for online and offline path planning as well as 2D and 3D environments [14].

2.2 Genetic Algorithms in UAS Path Planning

Genetic algorithms (GAs) are prominent in UAS path planning due to their robustness and adaptability [15]. They generate high-quality solutions for optimization and search problems by utilizing bio-inspired operators such as mutation, crossover, and selection [16, 17]. Moreover, they are effective for both offline and online path planning, capable of exploring large search spaces and adapting to dynamic environments [18].
In offline path planning, GAs can optimize predetermined routes to ensure minimal energy consumption and maximum coverage [19]. In online scenarios, GAs dynamically re-route UAS in response to real-time changes and obstacles, ensuring continuous optimal performance [20]. This adaptability makes GAs particularly suited for applications requiring high levels of autonomy and resilience, enhancing the overall utility and performance of UASs in various operational contexts [21, 22].
Research has shown that GAs can be used to effectively handle the complexities of UAS path planning by exploring a wide range of potential solutions and avoiding local optima [14]. Enhancements to the basic GA, such as dual-population strategies and vibrational genetic algorithms have further improved their performance in UAS applications. For instance, dual-population GAs use additional populations to dynamically balance exploration and exploitation of the solution space [23]. Multi-frequency vibrational GAs introduce new mutation strategies to enhance solution diversity and prevent premature convergence [24].
GAs have also been applied to specific challenges in UAS path planning, such as the multiple traveling salesman problem (mTSP) in multi-UAS systems ensuring optimal flight paths in dynamic and uncertain environments [25]. The integration of GAs with other computational intelligence methods, like fuzzy logic and neural networks, has enhanced the adaptability and efficiency of UAS path planning algorithms [26].
The named studies highlight the versatility and effectiveness of GAs in UAS path planning, particularly in optimizing complex, real-time missions under various constraints [14]. GAs are suitable for both, online and offline path planning and are capable of delivering good results for multi-objective, complex, and computationally intensive tasks [14, 27].

2.3 Genetic Algorithms and Kriging

Kriging, a geostatistical interpolation method, is widely used for predicting spatially continuous variables from discrete (measured) data points [28]. It not only provides predictions but also the uncertainty associated with them, making it particularly useful in environmental monitoring where spatially correlated data is prevalent [29].
While the integration of GAs and Kriging for optimizing UAS routes in contaminated airspaces has not been explicitly conducted, similar methodologies have been explored in other domains. For instance, a study employed a Markov Decision Process (MDP) combined with Kriging to optimize Autonomous Underwater Vehicle (AUV) routes. This methodology aimed to find a feedback-based plan for AUVs to visit important locations to estimate spatiotemporal fields, using predictions and errors from Kriging to develop a reward function that balances high prediction errors and energy consumption [30].
Another relevant study by Mishra et al. [31] presents an algorithm called AdaPP for adaptive sampling using robots to estimate environmental fields in large survey areas. Their approach focuses on data collection within a time constraint to provide an approximation of the environmental field, demonstrating improved performance against conventional sampling paths. This highlights the potential of adaptive path planning techniques to enhance data collection efficiency and accuracy in dynamic environments.

The study by Blanchard and Sapsis [32] introduces a novel approach for anomaly detection in environment exploration using UAS. Their method leverages Bayesian optimization to guide the UAS toward regions of strong anomalies, emphasizing extremes in the environmental data. This approach is particularly relevant for applications requiring the detection of abnormal features, such as extreme topographic depressions or abnormal concentrations of chemical trace substances or radiation. The integration of informative path planning with anomaly detection provides a robust framework for environmental monitoring, especially under adverse conditions where prior beliefs about the environment may be imprecise or erroneous.
Both Mishra et al. and Blanchard and Sapsis utilized (Sparse) Gaussian Processes for environmental modeling and spatial prediction. These methods highlight the effectiveness of combining advanced statistical techniques with path planning algorithms. However, this paper will focus on using a GA in combination with Kriging. This approach leverages the robust optimization capabilities of GAs and the precise spatial prediction provided by Kriging to improve the accuracy and reliability of UAS path planning for environmental monitoring missions.

3. Methodology

This chapter outlines the methodology used to optimize route planning for in-situ measurements in contaminated airspace. It begins with a detailed description of the path finding setup, including the parameters and constraints relevant to the mission. Following this, the study's contamination scenario is presented, illustrating the use of the ICON-ART model for predicting the spread of contaminants such as volcanic ash and radionuclides. The chapter then delves into the Kriging approach for spatial interpolation, explaining how it is utilized to estimate contamination levels at unsampled locations. Finally, the optimization approach employing a genetic algorithm is discussed, highlighting its role in refining flight routes to minimize the mean absolute error (MAE) of Kriging estimates. Each section provides both theoretical background and practical implementation details to give a comprehensive understanding of the route optimization process.

3.1 Path Planning Setup

The primary objective of the path planning algorithm is to efficiently collect in-situ measurement data during a RPAS mission while adhering to mission parameters outlined in Table 1. This involves a multi-objective optimization process starting with pre-flight *route* design, initially without considering the vertical flight dimension in an initial step.

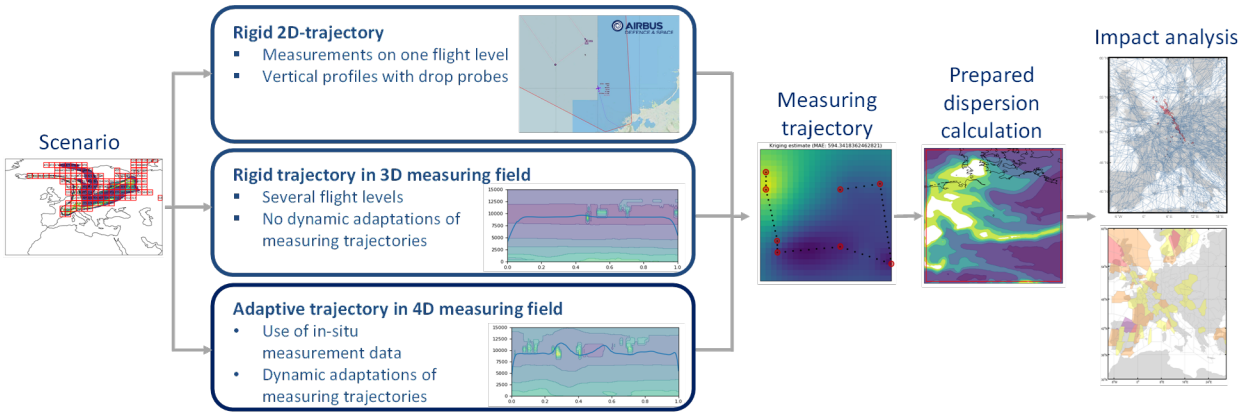

Figure 2 – Data flow and path planning setup for in-situ measurements and impact analysis.

The basic setup is visualized in Figure 2. It displays the data flow starting with a propagation calculation (Scenario), which serves as input for the path planning process. This path planning process can either be carried out with a i.) rigid 2D route on one selected flight level, ii.) a rigid route in a 3D measuring field, or it can iii.) consider the use of real-time in-situ measurement data as feedback for the dynamic route adaptation. The vertical profiles can basically also be measured using drop probes, which can be combined with the flight path generation. The complexity increases from an

offline 2D path planning problem to a 3D online path planning problem. The algorithm will generate a measuring route for the RPAS, which will lead to an updated propagation calculation and is finally used for the impact analysis through the identification of contaminated airspace. The methodology of the static pre-flight path planning will be discussed in this paper.

3.2 Contamination Scenario

The starting point of the path planning process is a propagation calculation provided by the DWD. The ICON-ART model, a DWD numerical weather prediction model, includes aerosols and reactive trace gases to forecast the propagation of natural airborne hazards such as volcanic ash, dust, and radionuclide clouds [33].

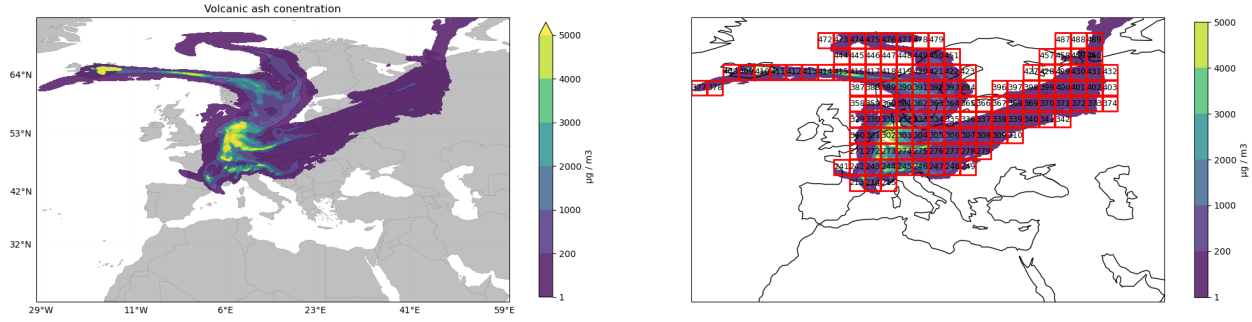

(a) ICON ART propagation calculation

(b) Division into grids for route planning

Figure 3 – Volcanic ash contamination 48h after eruption of Grimsvoetn at an altitude of approx. 1550m (left), grid for dividing the propagation area into individual maps for in-situ masurements (right).

Figure 3a shows the ICON-ART propagation calculation of DWD for the Grímsvötn volcano 48 hours after the eruption at an altitude of approximately 1550 meters. This dataset will be used to demonstrate the functionality of the proposed algorithm. The forecast model includes 90 dedicated height levels, which are not evenly distributed but vary based on spatial location and relative height concerning the earth's topology. For the selected level 80, the average height is approximately 1550 meters. It is assumed that the height within each subsection for the dimensions of a flight mission at the selected height level remains constant.

Figure 3b illustrates the division of the propagation calculation into gridded sections, referred to as maps (shown in red). Each grid, or map, contains 16 x 16 data points at the selected altitude level. These map sections are filtered to have at least an average concentration value of 1 μg/m^3 and 70% of concentration data points greater than zero. This threshold, as well as the number of measurement points per map, can be set manually and directly influence the number and size of the individual maps used for the subsequent generation of flight routes. This selection of spatial subsections is used to verify the path planning algorithm as well as its computational applicability. The latitudinal and longitudinal limits of the whole scenario, the full set of subsections, or just the borders of a single mission can be set.

At the stage of offline pre-flight path planning, the feedback to evaluate the quality of a measurement route consists of assumed measurements. These assumed measurements are interpolated using the four nearest surrounding points from the propagation calculation at an assumed measurement location. The evaluation of the measurement path is done by extrapolating the assumed measurements to the unknown areas and comparing these against the underlying data of the numerical contamination propagation, which served as input. The use of Kriging for this spatial interpolation is discussed in the next subsection.

3.3 Kriging for Spatial Interpolation

Kriging is a geostatistical method used to predict spatially continuous variables from discrete data points. It provides estimates at unmeasured locations based on surrounding values, effectively modeling spatially correlated data and offering predictions along with associated uncertainty measures

[34]. In this context, the Kriging estimate of the measuring field is calculated using a variogram based on the assumed set of waypoints and measurements from the propagation calculation.
The variogram is a fundamental tool in Kriging that describes the degree of spatial dependence of a spatial random field or stochastic process. It is defined as:

$$\gamma(h) = \frac{1}{2N(h)} \sum_{i=1}^{N(h)} [Z(s_i) - Z(s_i + h)]^2 \tag{1}$$

where $\gamma(h)$ represents the variogram value for lag h, $N(h)$ is the number of pairs of observations a distance h apart, $Z(s_i)$ is the value of the variable at location s_i, and $Z(s_i + h)$ is the value at location $s_i + h$ [35]. The variogram characterizes how the similarity between observations changes with distance. Ordinary Kriging uses this variogram to generate estimates at unsampled locations with an unknown mean and is used in this examination exclusively. The estimated value $\hat{Z}(s_0)$ at location s_0 is calculated as:

$$\hat{Z}(s_0) = \sum_{i=1}^{N} \lambda_i Z(s_i) \tag{2}$$

where λ_i are the Kriging weights, $Z(s_i)$ are the observed values, and $\hat{Z}(s_0)$ is the estimated value at location s_0. The Kriging weights λ_i are determined by solving the Kriging system:

$$\begin{aligned} &\sum_{j=1}^{N} \lambda_j \gamma(s_i - s_j) + \mu = \gamma(s_i - s_0) \quad \text{for } i = 1, \ldots, N \\ &\sum_{j=1}^{N} \lambda_j = 1 \end{aligned} \tag{3}$$

where $\gamma(s_i - s_j)$ is the variogram value between locations s_i and s_j, $\gamma(s_i - s_0)$ is the variogram value between s_i and the estimation location s_0, and μ is a Lagrange multiplier used to minimize estimation variance [34].
Kriging provides a robust method for spatial interpolation, allowing us to generate accurate estimates of contamination levels at unsampled locations using the spatial correlation structure described by the variogram. The implementation of [36] is used to generate the Kriging estimates, ensuring precise spatial predictions. However, to optimize the RPAS routes for in-situ measurements and minimize the MAE of these Kriging estimates, we leverage the strengths of a genetic algorithm. This combination enables us to refine the route for enhanced data collection and spatial prediction accuracy.

3.4 Genetic Algorithm for Route Optimization

A genetic algorithm is employed to optimize the route of RPAS for in-situ measurements. The goal is to reduce the MAE of the Kriging estimate compared to the original ICON-ART forecast data. The GA achieves this by evolving a population of candidate routes through the use of genetic operators such as selection, crossover, and mutation [16]. The algorithm's components and procedure are displayed as pseudo code in Algorithm 1, and the input parameters are described in Table 2.

Parameter	Description
Spatial Grid (M)	2D spatial field from ICON-ART propagation
Population size (N_{pop})	Number of routes in each generation
Number of generations (G)	Iterations of the algorithm
Initial route points (T)	Number of support route points
Crossover rate (P_c)	Probability of crossover between parents
Mutation rate (P_m)	Probability of mutation in offspring
Number of elites (E)	Number of top individuals carried to next generation
Selection method	Rank

Table 2 – Parameters of the Genetic Algorithm

Algorithm 1 RouteOptimization(T, M, N_{pop}, G, P_c, P_m, E)

Input: T {Initial route points}, M {2D spatial grid}, N_{pop} {Population size}, G {Number of generations}, P_c {Crossover rate}, P_m {Mutation rate}, E {Number of elites}
Output: best_individual {Optimized route}
Initialize population P with N_{pop} random routes from T
Evaluate fitness f of each individual in P using MAE from Kriging estimates
Initialize best_individual with the individual having the best fitness in P
for generation = 1 to G **do**
    Select parents from population P based on fitness f
    Apply crossover with rate P_c to generate offspring
    Apply mutation with rate P_m to offspring
    Find shortest path of initial route points using a 2-opt heuristic
    Interpolate points based on Map grid as pseudo measurements
    Evaluate fitness f of offspring using MAE from Kriging estimates
    Sort the combined population of current individuals and offspring by fitness
    Select top E individuals as elites for the next generation
    Select the rest of the next generation from the combined population excluding the elites
    Update best_individual if any individual has better fitness
end for
return best_individual

The initial population P of routes is generated randomly from the set of initial route points T, which act as supporting points within the 2D spatial grid M. This spatial grid is a section of the segmented scenario (spatial field), shown in Figure 3b, and will be referred to as the spatial grid or map.
To optimize the initial route points with respect to minimal travel distance, a 2-opt heuristic is used, ensuring efficient routes with minimal total distance. Further points are interpolated based on the spatial grid, serving as pseudo measurements to refine the Kriging estimation. The distance of these interpolated points is based on the sample distance of the initial spatial grid.
The fitness f of each route of the current generation G is evaluated based on the MAE between the Kriging estimates and the actual data from the spatial grid. Routes with lower MAE values receive higher fitness scores, indicating a closer match to the actual data. The fitness function is defined as:

$$f(\text{route}) = \frac{1}{n}\sum_{i=1}^{n}|y_i - \hat{y}_i| \tag{4}$$

where y_i are the observed values and $\hat{y}_i$ are the Kriging estimates.
For the generation of the Kriging estimates, an exponential variogram is used. While conducting a small survey on a small subset of spatial grids, it was found that the exponential variogram led to better estimation results than a linear variogram.
Selection is performed using the rank-based method, where routes are ranked according to their fitness scores, and selection probabilities are assigned based on these ranks. This method increases the likelihood that high-ranking (i.e., more successful) routes will contribute to the next generation, while lower-ranking routes are gradually phased out. This approach helps maintain diversity in the population and avoids premature convergence to local optima.
Crossover and mutation are genetic operators applied to generate new routes. Crossover combines segments of two parent routes to create offspring, introducing new combinations of waypoints. This is done by selecting a random index where the parents' waypoints are split and recombined, and is known as single-point crossover [37]. Mutation introduces random changes to some routes, where a single waypoint will be altered, promoting exploration of the solution space and helping to avoid local optima.
After applying selection, crossover, and mutation, the old generation of routes is replaced by the new generation. This cycle repeats over multiple generations, with the average fitness of the population typically increasing, indicating convergence towards an optimal solution.

Elitism is implemented in the genetic algorithm to ensure that the best-performing individuals are preserved in each generation. This technique involves selecting the top E individuals based on their fitness scores and directly carrying them over to the next generation. By doing so, elitism helps maintain high-quality solutions and prevents the loss of valuable genetic material over successive generations. This approach can accelerate convergence towards an optimal solution while maintaining robustness against premature convergence [38].
The fitness of the new offspring is reevaluated using the MAE from the Kriging estimates. The best individuals from the current population and the new offspring form the next generation. The route with the best fitness score is updated if any offspring have a better score.

4. Results

In this section, we present the findings from our study on optimizing RPAS routes for in-situ measurements of contaminated airspaces using Kriging and a genetic algorithm. Our results highlight the effectiveness of this combined approach in improving the measurement route by reducing the MAE of Kriging estimates.
We begin by detailing the initial setup and parameters used for the route optimization, followed by a comprehensive analysis of the genetic algorithm's performance across various scenarios. The ICON-ART propagation serves as the starting point of the examination, which is divided into subsections as shown in Figure 3b. These spatial grids (M) are the input for the RouteOptimization Algorithm 1. Additional parameters used for the generation of the routes in this results section are displayed in Table 3.
Next, we present the iterative process of the genetic algorithm, illustrating the improvement in Kriging estimates over successive generations. Example spatial grids will be discussed in detail to demonstrate the algorithm's effectiveness, although the algorithm converges for all sections. This is followed by a comparative analysis of the performance of the optimized routes against standard coverage patterns. Finally, we discuss the implications of our findings and potential areas for future research.

Parameter	Value
Population size (N_{pop})	50
Crossover rate (P_c)	0.7
Mutation rate (P_m)	0.2
Generations (G)	30
Initial route points (T)	6
Selection method	Rank
Variogram	Exponential
Elitism (E)	1

Table 3 – Calculation Parameters of the Genetic Algorithm.

Each iteration's population consists of 50 routes (N_{pop}), and the algorithm runs for a total of 30 generations (G). Each route is defined by six initial route points (T), forming the basis for waypoint generation and the interpolation of assumed measurement points. The crossover probability (P_c) between two routes is 0.7, while the mutation probability (P_m) is 0.2. Rank-based selection is used to preferentially select routes with higher fitness for reproduction, and one elite individual (E) is carried over to the next generation to ensure that the best solutions are retained.
Figure 4 illustrates the iteration process of the genetic algorithm, comparing reference data and Kriging estimates for Map 682 across different generations, using the MAE. The first row shows the reference data, while the second row presents Kriging estimates for different generations: (a) Generation 0, (b) Generation 7, and (c) Generation 15. The best individual (route) is displayed for each Generation.
At Generation 0, the initial Kriging estimate for Map 682 has a mean absolute error (MAE) of 91.88 and a total mission distance of 499.62 km. By Generation 7, the Kriging estimate shows a reduction in MAE to 72.80, with a corresponding decrease in total mission distance to 480.58 km, indicating effective optimization by the GA. By Generation 15, the MAE further decreases to 62.59, while the to-

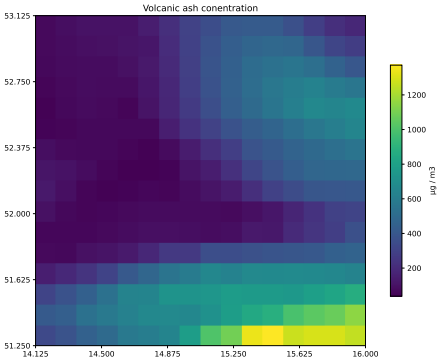

(a) Reference data (Map 682)

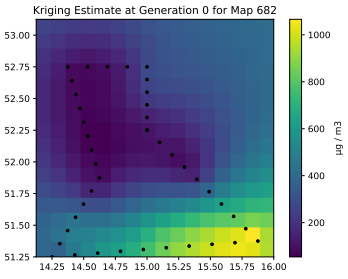

(b) Kriging estimate ($G = 0$)

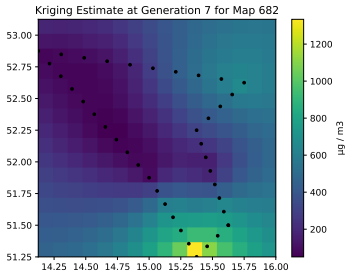

(c) Kriging estimate ($G = 7$)

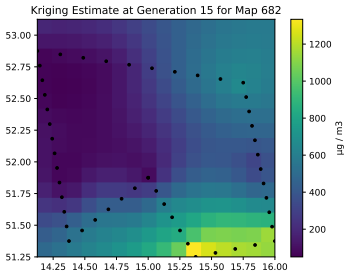

(d) Kriging estimate ($G = 15$)

Figure 4 – Comparison of reference data and Kriging estimates for Map 682. The first row shows the reference data, and the second row presents Kriging estimates for different Generations of the GA (G): (a) Generation 0, (b) Generation 7, and (c) Generation 15.

tal mission distance adjusts to 502.31 km, demonstrating continued improvement in Kriging estimate accuracy and refinement of the measurement route. The evolution of the fitness of the population, specifically showing the MAE of best route of each generation, is illustrated in Figure 5 for Map 682. Unlike the previous figure, which showcased only three selected generations, this figure depicts the convergence of the optimization process over multiple iterations. It is evident that the MAE decreases progressively throughout the iterations.

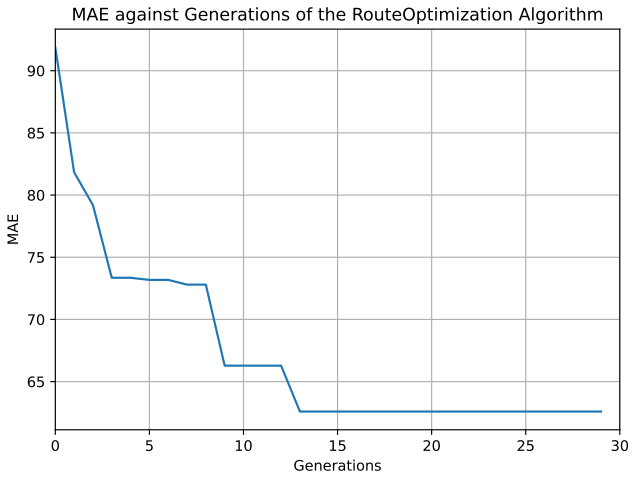

Figure 5 – MAE vs. Generations for the RouteOptimization Algorithm for Map 682

It is important to note that the total mission distance is not incorporated as a weighted factor in the fitness function nor as an excluding criterion during the optimization process. However, the initial

size of the spatial grid is strongly correlated with the total mission distance. In this initial approach, where detailed flight performance characteristics are not fully integrated and no comprehensive flight performance model is employed, it is evident that the MAE is significantly reduced while maintaining a comparable total mission distance. This finding highlights the algorithm's capacity to improve measurement accuracy effectively without substantially altering the overall mission length, thereby demonstrating its potential utility in practical applications where both accuracy and efficiency are critical.

The optimization algorithm demonstrates convergence and successfully generates routes for all subsets and spatial grids of the volcanic ash event as shown in Figure 3, although with varying accuracy based on the underlying field topology. Generally, the proposed algorithm effectively reduces the MAE and optimizes the measurement routes. The genetic algorithm adapts to different spatial grids, achieving different levels of optimization depending on the spatial field.

Performance Evaluation of Path Planning Methods

To evaluate the performance of the GA in route optimization, the algorithm was applied to one grid with a fixed set of initial route points. In this section, we extend the evaluation by varying the initial route points for the same spatial grid size. Additionally, we compare the GA with a standard pattern used in coverage path planning [39, 40], specifically the parallel search pattern, which systematically flies row or column-wise over the contaminated area.

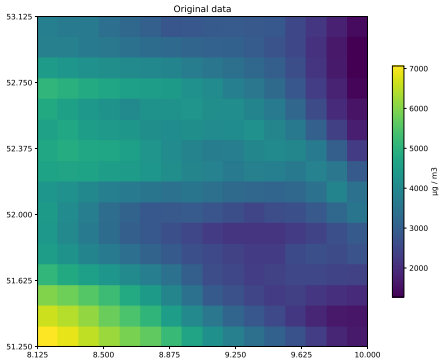

(a) Reference data (Map 679)

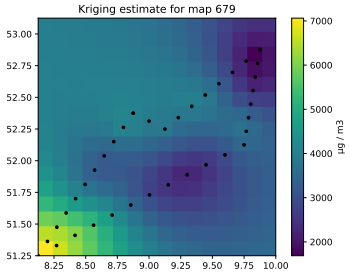

(b) Kriging estimate ($T = 5$)

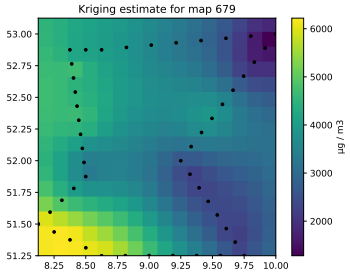

(c) Kriging estimate ($T = 8$)

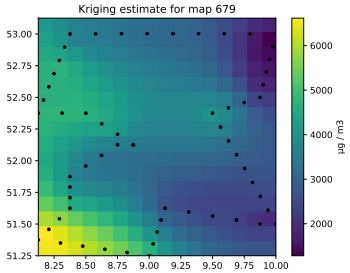

(d) Kriging estimate ($T = 15$)

Figure 6 – Comparison of reference data and Kriging estimates for Map 273. The first row shows the reference data, and the second row presents Kriging estimates for different initial route points (T): (a) 5 points, (b) 8 points, and (c) 15 points.

Figure 6 presents a detailed comparison between the reference data and the Kriging estimates generated using the genetic algorithm for Map 679. Figure 6a displays the reference data for Map 679, serving as the baseline for comparison. Figures 6b, 6c, and 6d show the Kriging estimates for different initial route points (T), specifically for 5, 8, and 15 points, respectively. Each displayed route is overlaid on top of the Kriging estimate based on these assumed measurement points (the route points). With an increased number of initial route points, more area is covered by the route, en-

hancing the Kriging estimate's accuracy. This improvement is graphically visible when comparing the Kriging estimates with the reference data and will be further discussed in the comparative analysis.

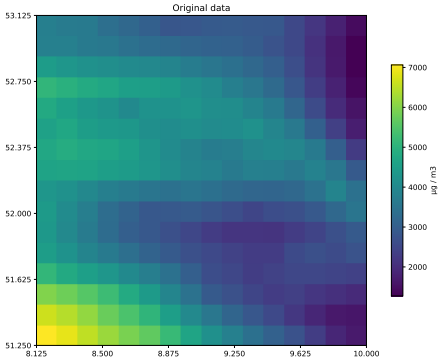

(a) Reference data (Map 679)

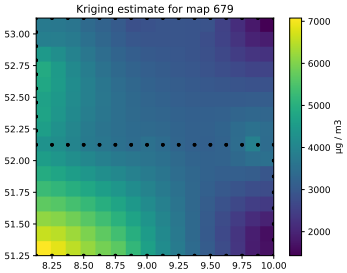

(b) Kriging estimate (3 rows)

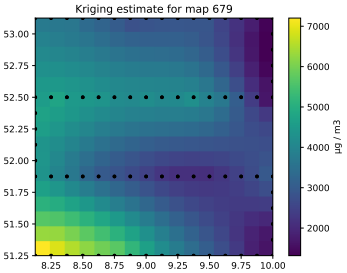

(c) Kriging estimate (4 rows)

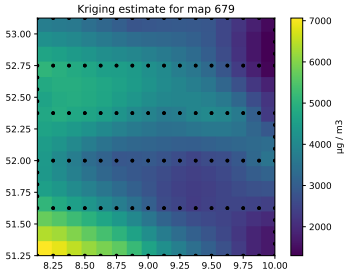

(d) Kriging estimate (6 rows)

Figure 7 – Comparison of reference data and Kriging estimates for Map 273 using the lawnmower method. The top row shows the reference data, and the bottom row presents Kriging estimates for different numbers of rows: (a) 10 rows, (b) 15 rows, and (c) 25 rows.

Figure 7 provides a comprehensive comparison between the reference data and the Kriging estimates obtained using the parallel search pattern for Map 679. The figure is organized similarly to the figure for the GA: Figure 7a displays the reference data for Map 679, serving as the baseline for comparison. Figures 7b, 7c, and 7d show the Kriging estimates for 3, 4, and 6 rows, respectively. These subfigures illustrate the performance of the parallel search pattern in terms of Kriging estimation accuracy. The results demonstrate how varying the number of rows affects the area coverage and estimation error. The performance improves with an increased number of rows, enhancing the coverage area and reducing the estimation error. This is again graphically visible as the Kriging estimate in Figure 7d represents the contamination reference better than the estimate based on three rows on the most left side. A detailed analytical comparison with the GA-generated routes will be discussed in the following, highlighting the differences in accuracy and efficiency between the methods.
The scatter plots in Figure 8 illustrate the Root Mean Squared Error (RMSE) against the total mission distance for the UAS path planning algorithms. Subfigure (a) shows the results for routes generated by the genetic algorithm with various initial route points, while subfigure (b) presents the results for routes generated using the parallel search pattern, annotated by the number of rows. In analyzing the results, it is evident that the genetic algorithm generally produces a lower RMSE compared to the parallel search pattern for the same total mission distance. This suggests that the genetic algorithm is more efficient in optimizing the path to reduce error. Furthermore, configurations with a higher number of initial route points or rows tend to achieve lower RMSE values, albeit at the cost of increased mission distance. This trend signifies a trade-off between accuracy and efficiency, indicating that higher accuracy (lower RMSE) requires covering more distance.

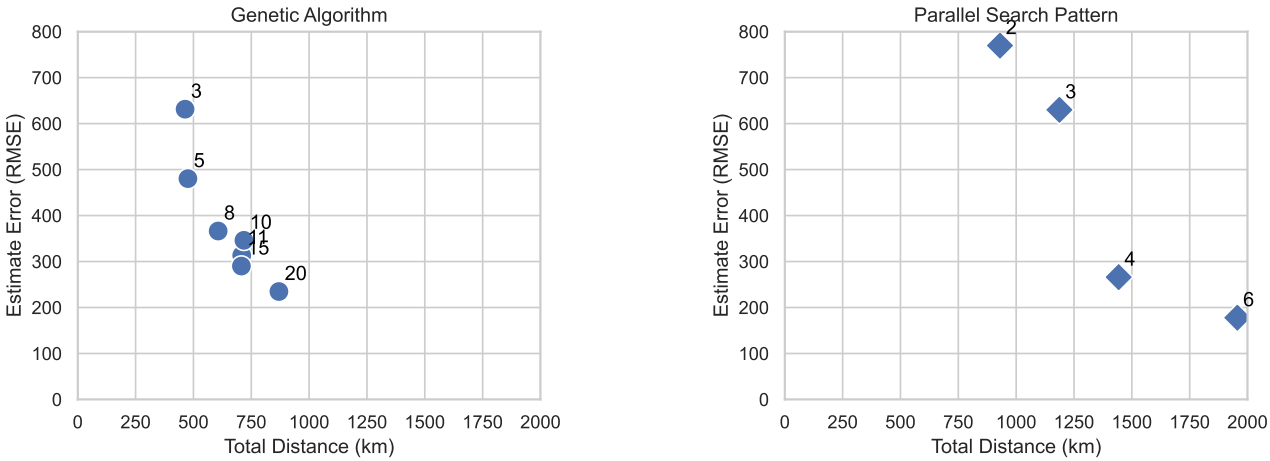

(a) Genetic Algorithm

(b) Parallel Search Pattern

Figure 8 – Estimate error vs. total mission distance by path planning method for map 679. (a) shows routes generated by the GA by the initial route points (annotated) and subfigure (b) shows routes generated using the parallel search pattern by the number of rows (annotated).

Given the approximate total mission distance of the RPAS is around 500 km as displayed in Table 1, it is clear that only routes generated by the GA fall within the range of the maximum mission distance. For instance, with 3 initial route points, the route by the GA achieves an RMSE of 631.37 with a total distance of 463.90 km. Meanwhile, the parallel search pattern with 3 rows achieves a similar RMSE of 629.95 but requires a significantly larger total distance of 1186.95 km. In comparison, the GA with 5 initial route points achieves an RMSE of 480.34 with a total distance of 476.16 km. While the total mission distance is slightly longer compared to the route generated with 3 initial route points, by approximately 2.6%, the RMSE is reduced by about 24%. This demonstrates that an advanced flight route exploring essential areas for the Kriging extrapolation can have a significant impact on the estimation without substantially increasing the total mission distance. This comparison highlights the efficiency of the genetic algorithm in optimizing the path.
When comparing 20 initial route points in the GA with 4 rows in the parallel search pattern, the GA achieves an RMSE of 234.80 with a total distance of 869.42 km, whereas the parallel search pattern achieves an RMSE of 266.03 but requires a total distance of 1443.05 km. The parallel search pattern is approximately 66% longer in total distance. Although the RMSE is better with the GA, the genetic algorithm covers a much shorter distance, making it a more practical option given the RPAS's maximum mission distance.
Overall, the genetic algorithm demonstrates a more balanced performance by providing reasonable RMSE values while maintaining a total mission distance within the operational range of the RPAS. This efficiency makes the GA a suitable choice for in-situ measurements, optimizing both accuracy and mission feasibility.

5. Conclusion and Outlook

This study presents a method for RPAS route planning using Kriging and a genetic algorithm to optimize in-situ measurements of contaminated airspaces. The integration of these methodologies has proven effective in reducing the MAE of Kriging estimates, providing a robust framework for improving UAS-based monitoring of atmospheric contamination events.
Future work will include conducting a parameter study to identify the optimal settings for genetic operators and evaluating the impact of adaptive iteration lengths and convergence monitoring on performance. Evaluating the robustness of the proposed method against unexpected measurements compared to the optimization basis, the spatial grid of the ICON-ART forecast, will be an important step. Evaluation of robustness using standard flight patterns for coverage path planning as well as a GA-optimized route with diverging measurements is a logical next step. The adaptation of the route optimization given the feedback of updated data emphasizes the step towards implementing

online, in-flight path planning adaptation and dynamic feedback mechanisms. This will allow the GA to dynamically adjust routes based on real-time data. Future work will also focus on evaluating the prediction of the contaminated airspace using different variogram models and their impact on the overall measuring performance.
These advancements will further improve the algorithm's ability to accurately and efficiently plan RPAS routes for atmospheric contamination monitoring, ensuring better utilization of RPAS capabilities and more accurate data collection.

6. Contact Author Email Address

Kuno.Buchtal@dlr.de
Alexander.Lau@dlr.de

7. Copyright Statement

References

[1] T. Bolić and Ž. Sivčev. Eruption of eyjafjallajökull in iceland: Experience of european air traffic management. *Transportation Research Record*, 2214(1):136–143, 2011.

[2] M. Hirtl et al. A volcanic-hazard demonstration exercise to assess and mitigate the impacts of volcanic ash clouds on civil and military aviation. *Natural Hazards and Earth System Sciences*, 20(6):1719–1739, 2020.

[3] H. Brenot et al. Eunadics-av early warning system dedicated to supporting aviation in the case of a crisis from natural airborne hazards and radionuclide clouds. *Natural Hazards and Earth System Sciences*, 21(11):3367–3405, 2021.

[4] M. Sangiorgi et al. The european radiological data exchange platform (eurdep): 25 years of monitoring data exchange. *Earth System Science Data*, 12(1):109–118, 2020.

[5] Airbus D&S. *DO-TP 25 – The Unmanned Airborne Testplatform*. Airbus D&S, 2022. Information brochure.

[6] Daniela Rojas Viloria, Elyn L. Solano-Charris, Andres Muñoz-Villamizar, and Jairo R. Montoya-Torres. Unmanned aerial vehicles/drones in vehicle routing problems: a literature review. *International Transactions in Operational Research*, 28(4):1626–1657, 2021.

[7] Colin C Murray and Alan G Chu. The flying sidekick traveling salesman problem: Optimization of drone-assisted parcel delivery. *Transportation Research Part C: Emerging Technologies*, 54:86–109, 2015.

[8] JA Guerrero and Y Bestaoui. Uav path planning for structure inspection in windy environments. *Journal of Intelligent and Robotic Systems*, 69(1–4):297–311, 2013.

[9] SH Teo, J Wang, L Geng, JYH Fuh, and YF Zhang. A heuristic mission planning algorithm for heterogeneous tasks with heterogeneous uavs. *Unmanned Systems*, 3(3):205–219, 2015.

[10] Sebastian M Ferrandez, Tim Harbison, Thomas Weber, Robert Sturges, and R Rich. Optimization of a truck-drone in tandem delivery network using k-means and genetic algorithm. *Journal of Industrial Engineering and Management*, 9(2):374–388, 2016.

[11] K Scott, R Dai, and M Kumar. Occlusion-aware coverage for efficient visual sensing in unmanned aerial vehicle networks. *IEEE Global Communications Conference*, pages 1–7, 2016.

[12] P Tokekar, JV Hook, D Mulla, and V Isler. Sensor planning for a symbiotic uav and ugv system for precision agriculture. *IEEE Transactions on Robotics*, 32(6):1498–1511, 2016.

[13] JYJ Chow. Dynamic uav-based traffic monitoring under uncertainty as a stochastic arc-inventory routing policy. *International Journal of Transportation Science and Technology*, 5(3):167–185, 2016.

[14] Y. Zhao, Z. Zheng, and Y. Liu. Survey on computational-intelligence-based uav path planning. *Knowledge-Based Systems*, 158:54–64, 2018.

[15] M Greiff and A Robertsson. Optimisation-based motion planning with obstacles and priorities. *IFAC-PapersOnLine*, 50(1):11670–11676, 2017.

[16] J. H. Holland. *Adaptation in Natural and Artificial Systems*. MIT Press, 1992.

[17] H Savuran and M Karakaya. Efficient route planning for an unmanned air vehicle deployed on a moving carrier. *Soft Computing*, 20(7):2905–2920, 2015.

[18] Y Bouzid, Y Bestaoui, and H Siguerdidjane. Quadrotor-uav optimal coverage path planning in cluttered environment with a limited onboard energy. *IEEE International Conference on Intelligent Robots and Systems*, pages 979–984, 2017.

[19] MA Russell and GB Lamont. A genetic algorithm for unmanned aerial vehicle routing. *Proceedings of the 7th Annual Conference on Genetic and Evolutionary Computation (GECCO'05)*, pages 1523–1530, 2005.

[20] J Chen, F Ye, and Y Li. Travelling salesman problem for uav path planning with two parallel optimization algorithms. *Progress in Electromagnetics Research Symposium*, pages 832–837, 2017.

[21] KK Lim, YS Ong, MH Lim, X Chen, and A Agarwal. Hybrid ant colony algorithms for path planning in sparse graphs. *Soft Computing*, 12(10):981–994, 2008.

[22] M Kim and ET Matson. A cost-optimization model in multi-agent system routing for drone delivery. *Communications in Computer and Information Science*, 772, 2017.

[23] T. Park and K. Ryu. A dual-population genetic algorithm for adaptive diversity control. *IEEE Transactions on Evolutionary Computation*, 14(6):865–884, 2010.

[24] Y. Pehlivanoglu. A new vibrational genetic algorithm enhanced with a voronoi diagram for path planning of autonomous uav. *Aerospace Science and Technology*, 16(1):47–55, 2012.

[25] O. Sahingoz. Flyable path planning for a multi-uav system with genetic algorithms and bezier curves. In *Proceedings of the 2013 International Conference on Unmanned Aircraft Systems (ICUAS)*, pages 41–48, 2013.

[26] Y. Wang, T. Wei, and X. Qu. Study of multi-objective fuzzy optimization for path planning. *Chinese Journal of Aeronautics*, 25(1):51–56, 2012.

[27] M. Bagherian and A. Alos. 3d uav trajectory planning using evolutionary algorithms: A comparison study. *The Aeronautical Journal (1968)*, 119:1271–1285, 2015.

[28] N. Cressie. The origins of kriging. *Mathematical Geology*, 22(3):239–252, 1990.

[29] G. Matheron. Principles of geostatistics. *Economic Geology*, 58(8):1246–1266, 1963.

[30] Gregory Murad Reis, Tauhidul Alam, Leonardo Bobadilla, and Ryan N. Smith. Feedback-based informative auv planning from kriging errors. In *2018 IEEE/OES Autonomous Underwater Vehicle Workshop (AUV)*, pages 1–6, 2018.

[31] Rajat Mishra, Mandar Chitre, and Sanjay Swarup. Online informative path planning using sparse gaussian processes. In *2018 OCEANS - MTS/IEEE Kobe Techno-Oceans (OTO)*, pages 1–5, 2018.

[32] A. Blanchard and T. Sapsis. Informative path planning for anomaly detection in environment exploration and monitoring. *Ocean Engineering*, 243, 2022.

[33] J. Schröter et al. Icon-art 2.1: a flexible tracer framework and its application for composition studies in numerical weather forecasting and climate simulations. *Geoscientific Model Development*, 11(10):4043–4068, 2018.

[34] Jean-Paul Chilès and Pierre Delfiner. *Geostatistics: Modeling Spatial Uncertainty*. John Wiley & Sons, 2009.

[35] Georges Matheron. Principles of geostatistics. *Economic geology*, 58(8):1246–1266, 1963.

[36] PyKrige Development Team. Pykrige: Kriging toolkit for python, 2020. Online; accessed 23-May-2024.

[37] Jonathan Shapiro. Genetic algorithms in machine learning. In Georgios Paliouras, Vangelis Karkaletsis, and Constantine D. Spyropoulos, editors, *Machine Learning and Its Applications: Advanced Lectures*, pages 146–168. Springer Berlin Heidelberg, Berlin, Heidelberg, 2001.

[38] Shumeet Baluja and Rich Caruana. Removing the genetics from the standard genetic algorithm. In *Machine Learning Proceedings 1995*, pages 38–46. Elsevier, 1995.

[39] Håvard Lægreid Andersen. Path planning for search and rescue mission using multicopters. Master's thesis, Institutt for teknisk kybernetikk, 2014.

[40] Tauã M. Cabreira, Lisane B. Brisolara, and Paulo R. Ferreira Jr. Survey on coverage path planning with unmanned aerial vehicles. *Drones*, 3(1), 2019.